Evaluation of rat C6 malignant glioma using spectral computed tomography

JIANLI LIU[1,2], JUNLIN ZHOU[2], JIE LI[3], LINGYAN ZHANG[2], PEILI ZHANG[2] and BIN LIU[1,3]

[1]The School of Nuclear Science and Technology, Lanzhou University, Lanzhou, Gansu 730000;
[2]Department of Radiology, Lanzhou University Second Hospital, Lanzhou, Gansu 730030;
[3]School of Stomatology, Lanzhou University, Lanzhou, Gansu 730000, P.R. China

Abstract. To investigate the use of multi-parameter spectral computed tomography (CT) for the evaluation of rat C6 glioma, 15 male Wistar rats were seeded with C6 glioma cells into the right basal ganglia and scanned 12 days later using spectral CT. Brain sections corresponding to scanned regions were immunostained for proliferation marker protein Ki67 (Ki67). Pearson's correlation coefficients between spectral CT parameters and Ki67 expression were determined. Thirteen rats survived 12 days and developed tumors. Optimal contrast-to-noise ratio achieved was 65 keV. Brain regions containing liquefactive necrosis, solid tumor, peripheral tumor and normal tissue differed significantly with regard to the spectral curve slope (0.24 ± 0.46, 1.81 ± 1.09, 0.8 ± 0.43 and 0.11 ± 0.27, respectively; $P < 0.01$), CT value (27.2 ± 4.51, 103.18 ± 35.48, 65.19 ± 13.72 and 38.07 ± 7.36, respectively; $P < 0.01$) and iodine concentration (2.41 ± 3.86, 16.05 ± 9.75, 6.76 ± 3.66 and 1.06 ± 2.35, respectively; $P < 0.0001$). The percentage of Ki67-positive cells correlated with the CT value ($r = 0.903$; $P < 0.001$), spectral curve slope ($r = 0.821$; $P < 0.001$) and iodine concentration ($r = 0.813$; $P < 0.001$). Spectral CT can detect microstructural changes within malignant gliomas and potentially provide important information regarding tumor proliferation and the extent of the invasion.

Introduction

Gliomas are the most common type of primary brain tumor seen in the clinic and account for around 80% of all malignant intracranial tumors (1). Although rare (the overall age-adjusted incidence rate is 4.67-5.73 per 100,000 persons), gliomas can cause substantial morbidity and mortality (1). Gliomas can

be subcategorized into four grades (I-IV) based on histopathological evaluation and clinical criteria (2), and those that proliferate aggressively (i.e., high grade) are associated with poor prognosis (3). Glioblastoma is a high-grade astrocytoma that shows invasive proliferation and has a poorly defined tumor edge (4). Microsurgical resection with adjuvant radiotherapy and chemotherapy is currently the treatment of choice for glioblastoma (5). However, glioblastoma is associated with a high relapse rate after surgery, and the median survival is only around 15 months (4,6). To optimize surgery, it is important that the extent of the tumor invasion within the brain is accurately evaluated before the operation is undertaken. In addition, the ability to determine tumor extent allows the response to treatment to be monitored accurately.

A variety of clinical imaging techniques are available for evaluating glioblastoma (5). Although computed tomography (CT) with contrast can identify certain features of a glioblastoma (which typically presents as a heterogeneous hyperdense ring with hypodense core), contrast-enhanced magnetic resonance imaging (MRI) remains the investigation of choice. In contrast-enhanced MR images, a glioblastoma typically appears as a contrast-enhanced mass with a ring of enhancement and a hypointense core of central necrosis. However, the tumor margins are often poorly defined in MRI sequences, and it can be difficult to distinguish tumor tissue from radiotherapy-induced non-specific changes in surrounding tissues. In addition, traditional or contrast CT and MRI provide little information on tumor grade. Magnetic resonance spectroscopy (which evaluates tissue metabolites) and dynamic susceptibility contrast MRI (which evaluates vascularity) can provide information regarding the aggressiveness or grade of a tumor, but these techniques have yet to gain widespread acceptance as standard imaging approaches for glioblastoma. Positron emission tomography (PET) with 2-fluoro-2-deoxy-D-glucose (FDG) is capable of assessing tumor cell metabolism, and its findings have been shown to correlate with histopathology results and disease course. Nonetheless, FDG-PET is an expensive imaging modality that has also failed to gain widespread acceptance. Thus, accurately evaluating a glioblastoma in the clinic, with a view to planning surgery or assessing treatment efficacy, remains challenging (7).

Single-source spectral CT is a relatively new technique that obtains dual-energy images by rapidly alternating

---

Correspondence to: Dr Bin Liu, The School of Nuclear Science and Technology, Lanzhou University, 199 Donggang West Road, Lanzhou, Gansu 730000, P.R. China
E-mail: lz8943115@qq.com

between two peak voltage settings. Spectral CT enables the reconstruction of monochromatic spectral images with energies ranging from 40 to 140 keV. Based on the values at any monochromatic energy of two known materials (water and iodine), the CT values can be calculated to obtain the density distribution, CT value distribution, Hounsfield unit (HU) curves and material-specific images; these data can be used for qualitative and quantitative analysis of material decomposition (8,9). An important advantage of spectral CT is that the selection of an appropriate monochromatic energy can reduce beam-hardening artifacts and optimize density resolution (8). Therefore, quantitative spectral CT is well suited to analyzing the biological features of the necrotic, solid and peripheral regions of a tumor and of adjacent normal tissues. Numerous studies (8-11) have demonstrated that spectral CT-based material decomposition can accurately distinguish and quantify a specific component from a mixture and reflect the blood supply of a tissue lesion. Furthermore, several investigations have reported that spectral CT shows promise as an imaging modality for pancreatic carcinoma (12), brain aneurysms (13) and liver tumors (14). However, to the best of our knowledge, no previous preclinical or clinical studies have assessed the utility of spectral CT for the evaluation of glioblastoma.

We hypothesized that spectral CT would provide useful information regarding glioblastoma margins, composition differences between various tumor regions, and tumor grade. Thus, the aim of the present preclinical study was to compare the results of spectral CT imaging with histopathological analyses in a rat model of glioblastoma in order to explore the potential of spectral CT for evaluating glioblastoma extent and grade. The rat C6 malignant glioma was used because it is similar to human glioblastoma in terms of tumor proliferation and biological behavior (WHO grade IV) and is considered a useful animal model for the study of imaging techniques (14). Another advantage of the rat C6 glioma is that it has a rich blood supply and thus shows strong enhancement and high tissue contrast resolution.

Materials and methods

Ethics statement. The study protocol was approved by the Ethics Committees of the Lanzhou University Second Hospital, Lanzhou, China (2015B-005).

Culture of C6 glioma cells. C6 glioma cells were purchased from the Cell Bank of the Shanghai Institute of Life Sciences, Chinese Academy of Sciences (Shanghai, China), and cultured in Dulbecco's modified eagle medium (DMEM; Gibco BRL, Grand Island, NY, USA) supplemented with 10% fetal bovine serum (FBS; Hyclone, Logan, UT, USA), 100 U/ml penicillin and 100 μg/ml streptomycin (Hyclone) at 37˚C with 5% CO_2.

Rat model of glioblastoma. All animal experiments were approved by the ethics committee of the No. 2 Hospital Affiliated to Lanzhou University (Lanzhou, China). Ten-week-old male Wistar rats (*n*=15) weighing 280-300 g were purchased from the Animal Experiment Center of Gansu College of Traditional Chinese Medicine (Lanzhou, China) and maintained in a standardized specific pathogen-free animal facility. Each rat was anesthetized by intraperitoneal injection

of 10% chloral hydrate (4 ml/kg) and fixed in a prone position on a murine stereotactic device. A 1-cm vertical incision was made at the lower right position along the sagittal direction, from the middle of the horizontal line between the eyes. A 0.6-mm-diameter drill was used to open the skull 1-mm above and 4-mm to the right of the bregma. A suspension of C6 cells (10 μl, 1.0×10^5 cells/μl) at the logarithmic growth phase was injected slowly (over a 5-min period) into the brain. The needle was slowly removed 5 min after the injection had finished. The incision was then sutured and sterilized. Subsequently, the rat was maintained as normal (15). C6 gliomas were observed to grow rapidly and reach a size of 2-4 mm at 12 days. Without intervention, rats bearing C6 gliomas usually die after 3-4 weeks; therefore, we chose to perform CT scanning on day 12 after tumor cell injection.

CT scanning. Twelve days after seeding of C6 cells, each rat was anesthetized with an intraperitoneal injection of 10% chloral hydrate (4 ml/kg) and fixed in a prone position. A disposable intravenous infusion needle (0.45x13.5 RWLB; Weigao Medical Polymer Co., Ltd., Weihai, China) was placed in the tail vein. Local CT scanning (HD750 CT scanner; GE Healthcare, Little Chalfont, UK) was performed first, followed by spectral CT scanning with a bolus injection of iohexol contrast agent (2.5 ml/kg, injected at 0.2 ml/s; Yangtze River Pharmaceutical Group, Taizhou, China). Scanning was performed in the axial mode, using the following parameters: gantry rotation time, 0.5 sec; tube voltage, 80/140 kVp, fast switching; tube current, 630 mAs; pitch, 1.375:1; detector coverage, 20 mm; scan field of view (SFOV), small head; display field of view (DFOV), 9 cm; reconstruction type, standard; matrix size, 512; adaptive statistical iterative reconstruction (ASIR), 30%; thickness, 0.625 mm; time delay, 30 sec.

Analysis of spectral CT data. Three-dimensional (3D) multiplanar reconstruction (MPR) images were generated using GSI general post-processing software running on an AW4.6 workstation (GE Healthcare). The maximal tumor length (including both the tumor and surrounding regions of suspected invasion) was measured perpendicular to the middle sagittal line, and the distance from the layer containing the maximal tumor length to the front of the brain was also determined. In the image layer (0.625 mm thick) containing the maximal tumor length, circular regions of interest (ROIs; diameter, 0.5 mm) were positioned at the following regions: the center of the solid tumor; a region of liquefactive necrosis; a peripheral tumor region; and adjacent normal brain tissue. Every region positioned 3 ROIs, and the average monoenergetic CT values and iodine concentrations were calculated for these regions. Two specialists experienced in the analysis of spectral CT data recorded the tumor diameter, distances from the ROIs in the peritumoral and adjacent brain tissue regions to the tumor center, CT values and iodine concentrations in a blinded fashion.

Histopathological analysis of tumor samples. After the completion of CT scanning, each rat was deeply anesthetized, fixed on a home-made surgical board and placed on a dissection plate. The chest was opened, the abdominal aorta was clamped, and the heart was exposed and isolated. A perfusion

needle was inserted into the left ventricular chamber and fixed in place using small-animal-specific forceps, and an incision was made in the right atrial appendage. The rat was first perfused with sterile saline (100 ml, 4°C) until the blood had been cleared (i.e., both lungs had turned white in color and the perfusate emerging from the right atrial appendage had become clear). Then, perfusion was continued with 4% para-formaldehyde (PFA; 100 ml, 4°C). The brain was collected by decapitation and fixed in PFA for 24 h.

Following fixation, the tumor section corresponding to the spectral CT layer was collected. The sample was dehydrated, embedded in paraffin, sectioned at 3-4 μm, and either stained with hematoxylin and eosin (HE) or immunostained for Ki67 (a marker of cell proliferation) using an anti-Ki67 primary antibody (1:180; Biorbyt, Wuhan, China) and an EnVision system in accordance with the manufacturer's instructions (Dako, Agilent Technologies, Santa Clara, CA, USA). The samples were developed using 3,3-diaminobenzidine (DAB) and re-stained with hematoxylin.

Two pathologists independently analyzed the pathological sections in a blinded manner. The tumor length was measured, and the percentage of Ki67-positive cells in each high-magnification field was calculated for regions corresponding to the ROIs selected in the CT scan. The tumor length included the tumor and surrounding area of infiltration (defined as the presence of a few tumor cells within normal brain tissue).

Statistical analysis. SPSS17.0 (SPSS Inc., Chicago, IL, USA) was used for the statistical analyses. The data are presented as the mean ± standard deviation (SD). The monoenergetic CT values, iodine concentration, effective atomic number and Ki67 expression intensity in the various regions (tumor center, peritumoral region, tumor-brain junction and adjacent brain tissue) were analyzed using one-way analysis of variance (ANOVA) with a least significant difference (LSD) post-hoc test. The correlation between each spectral CT parameter and Ki67 expression was analyzed using Pearson correlation analysis. P<0.05 was considered statistically significant.

Results

Optimizing the contrast-to-noise (CNR) ratio for spectral CT imaging. In order to identify the monochromatic energy that provided the optimal CNR, the CNR curve between tumor and adjacent brain tissue was plotted for monochromatic energies ranging from 40 to 140 keV. The optimal CNR was achieved at 65 keV in 11 of the 13 tumor-bearing rats (Fig. 1). In the remaining 2 rats, the optimal CNR was achieved at 60 keV and 70 keV, although good tissue contrast was also obtained at 65 keV in both these animals. Therefore, 65 keV was selected for monoenergetic imaging, 3D reconstruction and measurement of CT values.

Analysis of spectral CT imaging data. Of the 15 rats implanted with C6 glioma cells, 1 died 5 days after tumor seeding and 1 failed to develop a tumor (based on contrast-enhanced spectral CT imaging); these 2 animals were excluded from further analysis. A total of 13 rats showed successful development of a tumor mass in the right basal ganglion and were used for further study. The tumor diameter ranged from 1.4 to 3.8 mm.
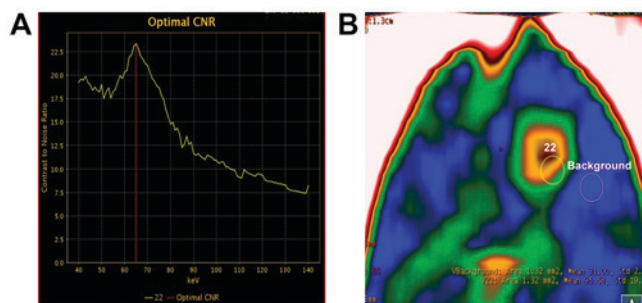

Figure 1. Selection of the best contrast-to-noise ratio (CNR) for displaying the glioma in spectral CT images. (A) The optimal CNR curve. The best resolution between the tumor and adjacent brain tissues was achieved at a monochromatic energy of 65 keV. (B) Sagittal monoenergetic pseudo-color images showing the sizes and positions (i.e., tumor, labeled '22', and adjacent brain tissue, labeled 'Background') of the regions of interest used to determine the optimal CNR curve.

Five of the 13 tumor-bearing rats had tumors with a diameter >2.5 mm. Enhanced spectral CT scanning of these 5 cases showed that a large tumor body and a substantial central area of liquefactive necrosis were evident in axial monoenergetic pseudo-color images at 65 keV. The solid tumor showed strong enhancement, and circular regions of uneven abnormal enhancement were visible around the tumor (Fig. 2A). The normalized spectral curves for the necrotic region, solid tumor, surrounding area of infiltration and normal brain tissue differed notably (Fig. 2B). The margins between the tumor, adjacent normal brain and skull were clearly evident in 3D reconstructed images (Fig. 2C).

For gliomas with a diameter <2.5 mm, axial monoenergetic pseudo-color images at 65 keV revealed that the center of the tumor showed strong enhancement. The enhancement decreased progressively from the tumor center to the peritumoral region, where a circular area with slightly higher CT value could be seen (Fig. 3A). The iodine-based material-decomposition images revealed that the tumor periphery contained circular regions with a slightly higher iodine concentration (Fig. 3B and C). The normalized spectral curves for solid tumor, peritumoral region and normal brain tissue differed notably (Fig. 3D). The iodine concentrations also differed between these regions (Fig. 3E), and a scatter plot of the iodine-water material decomposition allowed a clear distinction to be made between the tumor center, peritumoral region and adjacent brain tissue.

There were statistically significant differences between solid tumor, peritumoral region and normal brain tissue in the monoenergetic CT value, slope of the spectral curve and iodine concentration at 65 keV (P<0.001). The values for all 3 parameters were highest in solid tumor and lowest in normal brain tissue (Table I).

Histopathology. Gross inspection of all the pathological samples (*n*=13) showed that the brain structures were intact. Both the tumor and brain tissue were grayish in color, and the tumor was observed to have a small volume and distinct margin. Under low magnification, HE-stained sections of the solid region in the tumor center revealed a dense arrangement of tumor cells with irregular alignment (Fig. 4A) and substantial neovascularization (blue arrows in Fig. 4A). Fewer tumor
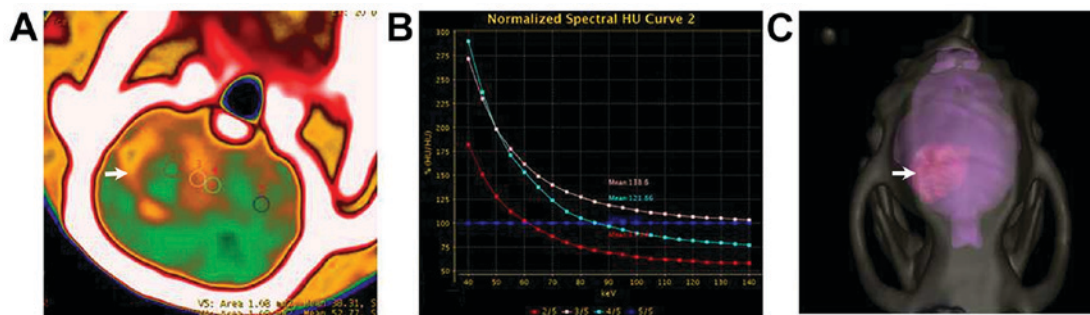
Figure 2. Enhanced spectral CT scanning of a rat C6 glioma with a diameter >2.5 mm. (A) Representative axial monoenergetic pseudo-color image at 65 keV. The tumor mass (arrow) contained a large area of liquefactive necrosis in its center. The solid tumor showed strong enhancement, while circular regions showing heterogeneous abnormal enhancement were visible around the tumor. (B) Normalized spectral Hounsfield unit (HU) curves derived from the spectral CT images. There were clear differences between the standardized curves for the necrotic region (red), solid tumor (pink), surrounding area of infiltration (green) and normal brain tissue (blue). (C) A representative 3D reconstructed image. The margins between the tumor (arrow) and the adjacent brain and skull are clearly evident.
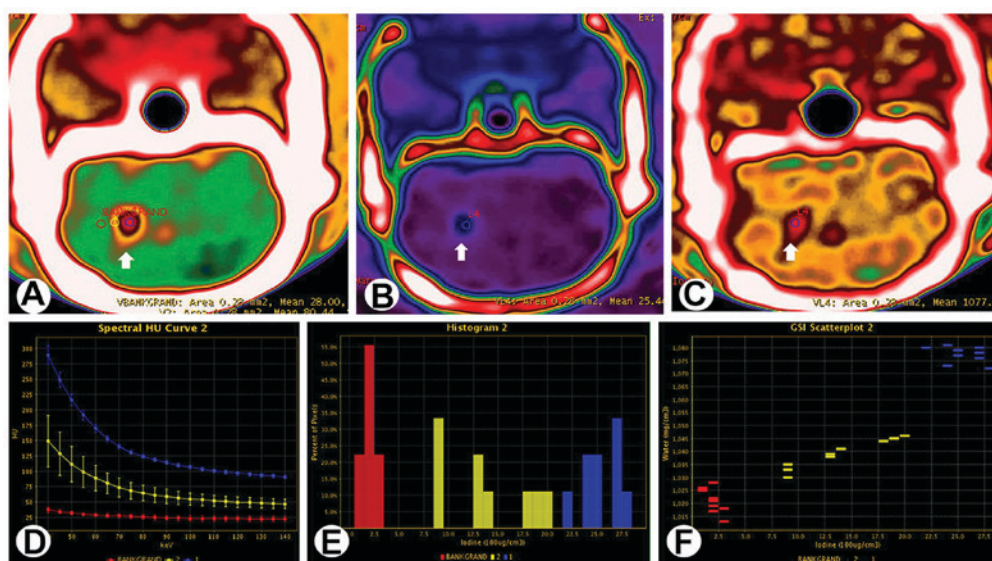

Figure 3. Enhanced spectral CT scanning of a rat C6 glioma with a diameter <2.5 mm. (A) Representative axial monoenergetic pseudo-color image at 65 keV showing a tumor with a diameter of 1.2 mm. The tumor center showed strong enhancement, and the degree of enhancement decreased progressively from the central to the peritumoral regions. At the peritumoral areas, circular regions with slightly higher CT values were evident. (B) The iodine-based material-decomposition images obtained using spectral CT showed circular areas of slightly higher iodine concentration in the peritumoral regions. (C) The water-based material-decomposition images showed that the water concentration in the tumor was higher. (D) Normalized spectral Hounsfield unit (HU) curves derived from the spectral CT images. There were noticeable differences between the standardized curves for the tumor center (blue), peritumoral region (yellow) and normal brain tissue (red). (E) Histogram of the iodine concentration at different regions. There were clear differences in the iodine concentration between the tumor center (blue), peritumoral region (yellow) and adjacent brain tissue (red). (F) Scatter plot of the iodine-water material decomposition. The differences between the iodine and water concentrations facilitated the distinction between the tumor center (blue), peritumoral region (yellow) and adjacent brain tissue (red). The white arrows in A-C indicate the tumor position.

cells and less neovascularization were present in the peritumoral region than in the central region (Fig. 4B). Under high magnification, the tumor cells were observed to have large nuclei, commonly atypical and mitotic. Immunostaining for Ki67 revealed that areas of liquefactive necrosis contained only a small number of Ki67-positive cells (i.e., nuclei stained deep brown; Fig. 4C). In contrast, the percentage of Ki67-positive cells in solid tumor regions exceeded 60% (Fig. 4D, upper left). A small number of Ki67-positive cells were also seen in peritumoral regions (Fig. 4D, lower right).

Correlation between spectral CT imaging results and histopathology data. Tumor diameter on day 12 after seeding of C6 glioma cells measured by spectral CT (2.39±0.66 mm) was not

significantly different to that measured from HE-stained histopathology specimens (2.41±0.71 mm; P=0.549). As shown in Table II, Ki67 expression correlated strongly with the CT value at 65 keV (correlation coefficient r=0.903, P<0.001, Fig. 5), the slope of the spectral curve (r=0.821, P<0.001, Fig. 5), and the iodine concentration (r=0.813, P<0.001).

Discussion

To the best of our knowledge, this is the first study to investigate the utility of spectral CT scanning for evaluating malignant glioma. The main findings of the present study were that spectral CT imaging was capable of identifying a C6 glioma in rat brain, delineating the tumor margins, and

Table I. Comparison of spectral CT-derived parameters (at 65 keV) and Ki67 expression (immunohistochemistry) between normal brain tissue and various tumor regions in a rat C6 malignant glioma model.

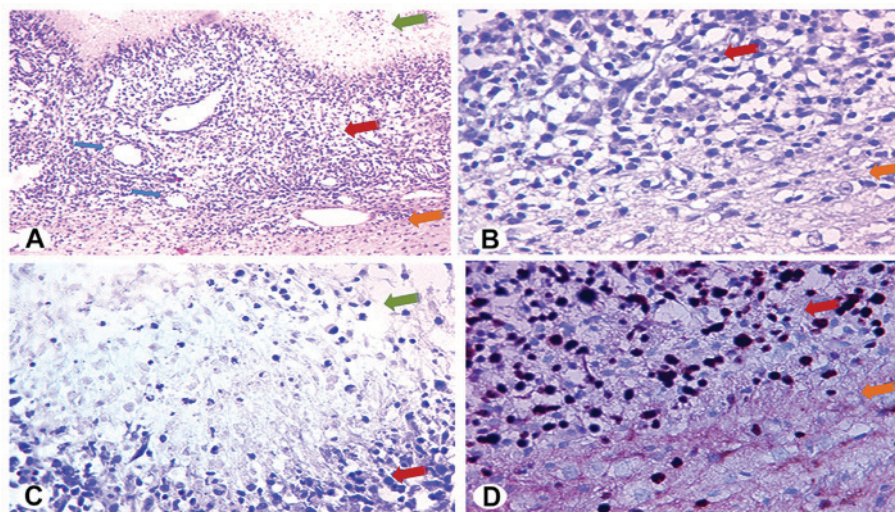| Parameters	Solid tumor region (n=13)	Peritumoralregions (n=13)	Normal brain tissue (n=13)	Liquefactive necrosis (n=5)	F	P-value
CT value	103.18±35.48	65.19±13.72	38.07±7.36	27.2±4.51	47.915	<0.001
HU curve slope	1.81±1.09	0.8±0.43	0.11±0.27	0.24±0.46	21.726	<0.001
Iodine conc.	16.05±9.75	6.76±3.66	1.06±2.35	2.41±3.86	15.174	<0.001
Ki67 (%)	60.77±12.39	26.54±6.89	1.7±0.32	10.00±3.54	175.364	<0.001

Figure 4. Histopathology of a rat C6 glioma. (A) Representative section of a tumor stained with hematoxylin and eosin (x100). (B) Representative section showing solid tumor and peritumoral region, stained with hematoxylin and eosin (x200). (C) Representative section of liquefactive necrosis within a tumor, immunostained for Ki67 (x200). (D) Representative section showing solid tumor and peritumoral region, immunostained for Ki67 (x400). Green arrows indicate liquefactive necrosis; red arrows indicate solid tumor; yellow arrows indicate an area of tumor cell infiltration; and blue arrows indicate neovascularization. (Images are representative of n=13).

differentiating between normal brain tissue and various tumor regions (solid tumor, area of liquefactive necrosis and peritumoral region). Furthermore, 3 parameters measured using spectral CT scanning (CT value, slope of the spectral curve and iodine concentration) correlated with Ki67 expression (a marker of cell proliferation) determined from histopathology studies. These results suggest that spectral CT scanning could potentially be used to improve the evaluation of glioblastoma and provide useful information regarding the extent and grade of the tumor.

Routine CT scans measure the decay of mixed-energy X-rays that penetrate the tissues to be tested, but the limitations of polychromatic X-rays, including beam-hardening effects, can sometimes make it difficult to distinguish a lesion from surrounding normal tissue (11). Spectral CT allows the generation of monochromatic spectral images with energies ranging from 40 to 140 keV and permits material-specific analysis that provides multi-parameter quantitative and qualitative data. An important advantage of monoenergetic spectral CT is that it effectively removes beam-hardening artifacts and therefore more accurately reflects changes in tissue density (8). It is thought that spectral CT is more sensitive at distinguishing structural differences within tissues and thus can facilitate the diagnosis of a tumor by providing richer

imaging information (8). However, no previous investigations have assessed whether the monoenergetic imaging and material-specific analysis provided by spectral CT can accurately reflect compositional changes within a brain glioma and whether the pathological basis of these changes is related to tumor cell proliferation, invasion or apoptosis. Therefore, the present preclinical study was carried out to explore whether monoenergetic spectral CT imaging and material-specific quantitative analysis could be used to detect malignant glioma cell infiltration and apoptosis. The rat C6 glioma was chosen for use in the animal model because it is similar to human glioblastoma in terms of growth and biological behavior and is widely used in imaging and interventional studies of malignant brain gliomas (14,15).

X-ray decay possesses distinct features at different energy levels. Low-energy X-rays have low penetrative ability and generate images with good contrast but high noise, while high-energy X-rays have high penetrative ability and generate images with low beam-hardening artifacts but low tissue contrast. Therefore, the energy level needs to be selected according to requirements (11,16). Patel and colleagues (17) reported that low-energy images increased the contrast between a pancreatic lesion and surrounding tissue and concluded that 50-52 keV was optimal for the display and

Table II. Pearson correlation analysis of the relation between Ki67 expression (immunohistochemistry) and spectral CT-derived parameters measured in normal brain tissue and various tumor regions (liquefactive necrosis, solid tumor, peripheral tumor).

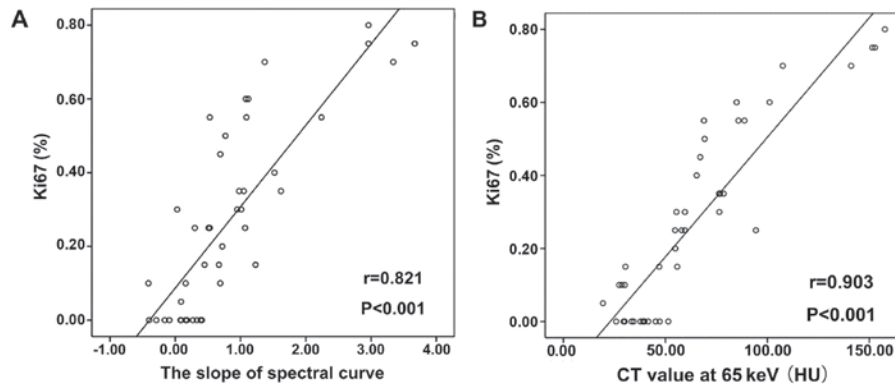| Parameters	Mean	Standard deviation	Correlation coefficient	P-value
Ki67 expression	0.2693	0.25614		
CT value at 65 keV	64.0839	35.29587	0.903	<0.001
Slope of the spectral curve	0.8264	0.95265	0.821	<0.001
Iodine conc. (100 μg/cm^3)	7.3286	8.4248	0.813	<0.001

Figure 5. Analysis of the correlations between Ki67 expression and parameters measured using spectral CT. (A) Pearson correlation analysis of the association between Ki67 expression and the slope of the spectral curve. (B) Pearson correlation analysis of the association between Ki67 expression and the CT value at 65 keV (HU).

diagnosis of pancreatic cancer. Tang and coworkers (18) compared abdominal images obtained with spectral CT and regular CT and concluded that monoenergetic spectral CT was better at delineating the gastrocolic ligament; the optimal CNR was at 50-70 keV. Hu *et al* (12) constructed a CNR curve for monochromatic energies ranging from 40 to 140 keV and determined that the optimal CNR for imaging pancreatic carcinoma xenografts was obtained at 70 keV. In our study, we used a similar approach to that of Hu and colleagues and determined that the optimal CNR for distinguishing glioma from normal brain tissue was obtained at 65 keV. Therefore, 65 keV was selected as the energy level for subsequent spectral CT imaging studies.

At 65 keV, the monoenergetic CT images of C6 glioma obtained in our study demonstrated stratification from the center to the periphery of the tumor. Spectral CT showed a low-density area of liquefactive necrosis within the tumor in all 5 cases where the tumor diameter was >2.5 mm. In the 8 cases with a tumor diameter <2.5 mm, a high-density, evenly distributed shadow was observed in the tumor center. In all cases, a circular shadow of slightly higher density could be seen in the peritumoral region. The tissue density in contrast-enhanced CT is largely dependent on the local concentration of the contrast agent and on tissue cell density (19). Since contrast agents cannot cross the intact blood-brain barrier, we speculate that tumor cell infiltration into the peritumoral area impairs part of the blood-brain barrier and/or induces abnormal neovascularization. The stratification observed from the center to the periphery of the tumor in CT images may have resulted from differences between the various regions in cell density, the degree of neovascularization and/or the extent

of blood-brain barrier impairment. Histopathological analysis (HE staining) revealed a sparse distribution of cells in areas of liquefactive necrosis but a dense distribution of cells with rich neovascularization in solid tumor regions. A small amount of tumor cell infiltration and abnormal neovascularization were evident in the peritumoral region, suggesting that variations in the monoenergetic CT values were associated with tumor cell density and microenvironment. Furthermore, the mean tumor size (including peritumoral region) measured with spectral CT imaging was consistent with that measured using histopathological techniques. Thus, monoenergetic CT images at 65 keV were able to accurately detect the extent of tumor infiltration.

Spectral CT demonstrated low-density liquefactive necrosis in all tumors with a diameter <2.5 mm. Histopathology with HE staining revealed that necrotic tissue debris and fluid were the major components of these areas, while the percentage of Ki67-positive cells was <10%. Moreover, lower CT values on spectral CT corresponded with increased severity of liquefactive necrosis. Liquefactive necrosis was not observed when the tumor size was <2.5 mm, and histopathology indicated that these tumors had been growing rapidly. It is likely that liquefactive necrosis arises when a C6 glioma reaches a certain size that results in an insufficient blood supply to the central portions of the tumor. Importantly, the presence of liquefactive necrosis could be sensitively detected by spectral CT.

We utilized spectral CT analytical software to measure the monoenergetic CT values at 40-140 keV in liquefactive, solid and peritumoral regions of the tumor as well as in normal brain tissue, and the slopes of the spectral curves were calculated. There were significant differences between regions in the slope of the spectral curve and the mean monoenergetic CT value.

The values for both parameters were highest in solid tumor, lowest in normal brain tissue, and intermediate in the peritumoral region. The absorption of X-rays at different energy levels varies for materials of differing compositions, allowing spectral CT to detect changes in local tissue structures and their microenvironment and analyze tumor cell proliferation and invasion (20,21). In our study, there was a strong and significant correlation between the slope of the spectral curve and Ki67 expression detected using immunohistochemistry. Ki67 expression is a widely accepted method for measuring the proliferative activity of malignant glioma cells (22): the higher the percentage of Ki67-positive cells in the tumor, the higher the mitosis rate and the greater the invasiveness of the tumor. Therefore, we hypothesize that the slope of the spectral curve could be used to indirectly reflect the proliferation and necrosis of malignant glioma as well as accurately measure the extent of tumor infiltration into surrounding tissues.

Based on the material decomposition images, we plotted the contrast agent distribution by detecting differences in iodine concentration. This approach can demonstrate local changes in tissue blood perfusion, which can facilitate the differential diagnosis of diseases with similar imaging features (23), including lung cancer (24). Aoki *et al* (24) analyzed the iodine concentrations in 57 cases of lung cancer and found that iodine concentration was tightly associated with CT perfusion parameters (blood flow, volume and blood vessel permeability) and could replace CT perfusion in the evaluation of local blood perfusion. Iodine concentration in contrast-enhanced CT was determined by the local concentration of contrast agent and was not affected by the gas composition of the tumor.

The iodine concentration in our study differed significantly between the various tumor regions, and associated with ki67 expression (P<0.001). Solid tumor regions had more intensive tumor cells, obvious karyokinesis, and significantly higher the iodine concentration and ki67 expression than other regions. Therefore, we believe that areas containing actively proliferating tumor cells have increased local blood flow and greater vascular permeability. Comprehensive analysis of the monoenergetic CT value, slope of the spectral curve and iodine concentration could be an effective method for detecting tumor cell proliferative activity, invasion and infiltration.

This study has certain limitations. First, the sample size was relatively small (*n*=13). Second, the lesion size was small; although a small ROI was selected with a diameter of 0.5 mm, there still may have been a degree of variation due to the volume effect. Third, spectral CT analysis was only performed on rat C6 gliomas, hence the generalizability of our observations to malignant gliomas in other species, including human patients, remains to be established. Fourth, direct comparisons between spectral CT and other imaging methods were not made. Additional preclinical and clinical studies with larger sample sizes are merited to further validate our findings.

In a rat model of malignant glioma, spectral CT multi-parameter analysis can distinguish between solid tumor, liquefactive necrosis, peritumoral regions and normal brain tissue, and effectively detect the infiltration of tumor into surrounding brain tissues. In particular, the monoenergetic CT value, slope of the spectral curve and iodine concentration all correlated with the percentage of Ki67-positive cells, which reflects the proliferative activity of tumor cells. Quantitative spectral CT analysis can potentially provide important imaging information for the dynamic monitoring of microstructural changes within malignant gliomas.

References

1. Ostrom QT, Bauchet L, Davis FG, Deltour I, Fisher JL, Langer CE, Pekmezci M, Schwartzbaum JA, Turner MC, Walsh KM, *et al*: The epidemiology of glioma in adults: A 'state of the science' review. Neuro Oncol 16: 896-913, 2014.
2. Louis DN, Ohgaki H, Wiestler OD, Cavenee WK, Burger PC, Jouvet A, Scheithauer BW and Kleihues P: The 2007 WHO classification of tumours of the central nervous system. Acta Neuropathol 114: 97-109, 2007.
3. Hayes J, Thygesen H, Droop A, Hughes TA, Westhead D, Lawler SE, Wurdak H and Short SC: Prognostic microRNAs in high-grade glioma reveal a link to oligodendrocyte precursor differentiation. Oncoscience 2: 252-262, 2014.
4. Wen PY, Macdonald DR, Reardon DA, Cloughesy TF, Sorensen AG, Galanis E, Degroot J, Wick W, Gilbert MR, Lassman AB, *et al*: Updated response assessment criteria for high-grade gliomas: Response assessment in neuro-oncology working group. J Clin Oncol 28: 1963-1972, 2010.
5. Young RM, Jamshidi A, Davis G and Sherman JH: Current trends in the surgical management and treatment of adult glioblastoma. Ann Transl Med 3: 121, 2015.
6. Stupp R, Mason WP, van den Bent MJ, Weller M, Fisher B, Taphoorn MJ, Belanger K, Brandes AA, Marosi C, Bogdahn U, *et al*: Radiotherapy plus concomitant and adjuvant temozolomide for glioblastoma. N Engl J Med 352: 987-996, 2005.
7. Kalpathy-Cramer J, Gerstner ER, Emblem KE, Andronesi OC and Rosen B: Advanced magnetic resonance imaging of the physical processes in human glioblastoma. Cancer Res 74: 4622-4637, 2014.
8. McCollough CH, Leng S, Yu L and Fletcher JG: Dual- and multi-energy CT: Principles, technical approaches, and clinical applications. Radiology 276: 637-653, 2015.
9. Ogata T, Ueguchi T, Yagi M, Yamada S, Tanaka C, Ogihara R, Isohashi F, Yoshioka Y, Tomiyama N, Ogawa K and Koizumi M: Feasibility and accuracy of relative electron density determined by virtual monochromatic CT value subtraction at two different energies using the gemstone spectral imaging. Radiat Oncol 8: 83, 2013.
10. Graser A, Johnson TR, Chandarana H and Macari M: Dual energy CT: Preliminary observations and potential clinical applications in the abdomen. Eur Radiol 19: 13-23, 2009.
11. Pomerantz SR, Kamalian S, Zhang D, Gupta R, Rapalino O, Sahani DV and Lev MH: Virtual monochromatic reconstruction of dual-energy unenhanced head CT at 65-75 keV maximizes image quality compared with conventional polychromatic CT. Radiology 266: 318-325, 2013.
12. Hu S, Huang W, Chen Y, Song Q, Lin X, Wang Z and Chen K: Spectral CT evaluation of interstitial brachytherapy in pancreatic carcinoma xenografts: Preliminary animal experience. Eur Radiol 24: 2167-2173, 2014.
13. Wang Y, Gao X, Lu A, Zhou Z, Li B, Sun X and Zhu B: Residual aneurysm after metal coils treatment detected by spectral CT. Quant Imaging Med Surg 2: 137-138, 2012.
14. Barth RF and Kaur B: Rat brain tumor models in experimental neuro-oncology: The C6, 9L, T9, RG2, F98, BT4C, RT-2 and CNS-1 gliomas. J Neurooncol 94: 299-312, 2009.
15. Liao J, Xia R, Liu T, Feng H, Ai H, Song B and Gao F: In vivo dynamic monitoring of the biological behavior of labeled C6 glioma by MRI. Mol Med Rep 7: 1397-1402, 2013.
16. Yamada Y, Jinzaki M, Tanami Y, Abe T and Kuribayashi S: Virtual monochromatic spectral imaging for the evaluation of hypovascular hepatic metastases: The optimal monochromatic level with fast kilovoltage switching dual-energy computed tomography. Invest Radiol 47: 292-298, 2012.

17. Patel BN, Thomas JV, Lockhart ME, Berland LL and Morgan DE: Single-source dual-energy spectral multidetector CT of pancreatic adenocarcinoma: Optimization of energy level viewing significantly increases lesion contrast. Clin Radiol 68: 148-154, 2013.
18. Tang L, Zhang XP, Sun YS, Li YL, Li XT, Cui Y and Gao SY: Spectral CT in the demonstration of the gastrocolic ligament: A comparison study. Surg Radiol Anat 35: 539-545, 2013.
19. Lusic H and Grinstaff MW: X-ray-computed tomography contrast agents. Chem Rev 113: 1641-1666, 2013.
20. Li A, Liang H, Li W, Wang Z, Pang T, Li J, Shi H and Zhang C: Spectral CT imaging of laryngeal and hypopharyngeal squamous cell carcinoma: Evaluation of image quality and status of lymph nodes. PLoS One 8: e83492, 2013.
21. Wu LM, Li YL, Yin YH, Hou GQ, Zhu R, Hua XL, Xu JR and Chen ZA: Usefulness of dual-energy computed tomography imaging in the differential diagnosis of sellar meningiomas and pituitary adenomas: Preliminary report. PLoS One 9: e90658, 2014.
22. Sun H, Guo D, Su Y, Yu D, Wang Q, Wang T, Zhou Q, Ran X and Zou Z: Hyperplasia of pericytes is one of the main characteristics of microvascular architecture in malignant glioma. PLoS One 9: e114246, 2014.
23. Yu Y, He N, Sun K, Lin X, Yan F and Chen K: Differentiating hepatocellular carcinoma from angiomyolipoma of the liver with CT spectral imaging: A preliminary study. Clin Radiol 68: e491-e497, 2013.
24. Aoki M, Takai Y, Narita Y, Hirose K, Sato M, Akimoto H, Kawaguchi H, Hatayama Y, Miura H and Ono S: Correlation between tumor size and blood volume in lung tumors: A prospective study on dual-energy gemstone spectral CT imaging. J Radiat Res 55: 917-923, 2014.